nature cell biology

Filamin-A regulates actin-dependent clustering of HIV receptors

Sonia Jiménez-Baranda[1], Concepción Gómez-Moutón[1], Ana Rojas[2,6], Lorena Martínez-Prats[3], Emilia Mira[1], Rosa Ana Lacalle[1], Alfonso Valencia[2,6], Dimiter S. Dimitrov[4], Antonella Viola[5], Rafael Delgado[3], Carlos Martínez-A.[1] and Santos Mañes[1,7]

Human immunodeficiency virus (HIV)-1 infection requires envelope (Env) glycoprotein gp120-induced clustering of CD4 and coreceptors (CCR5 or CXCR4) on the cell surface; this enables Env gp41 activation and formation of a complex that mediates fusion between Env-containing and target-cell membranes[1]. Kinetic studies show that viral receptors are actively transported to the Env-receptor interface in a process that depends on plasma membrane composition and the actin cytoskeleton[2–7]. The mechanisms by which HIV-1 induces F-actin rearrangement in the target cell remain largely unknown. Here, we show that CD4 and the coreceptors interact with the actin-binding protein filamin-A, whose binding to HIV-1 receptors regulates their clustering on the cell surface. We found that gp120 binding to cell receptors induces transient cofilin-phosphorylation inactivation through a RhoA–ROCK-dependent mechanism. Blockade of filamin-A interaction with CD4 and/or coreceptors inhibits gp120-induced RhoA activation and cofilin inactivation. Our results thus identify filamin-A as an adaptor protein that links HIV-1 receptors to the actin cytoskeleton remodelling machinery, which may facilitate virus infection.

To understand the mechanism by which Env binding induces F-actin rearrangement in target cells, we sought to identify host-cell proteins that interact with the primary HIV-1 receptor, CD4. A yeast two-hybrid screen of a Jurkat T cell line cDNA expression library was performed using the CD4 intracellular domain ($CD4^{IC}$) as bait. Sequencing of positive clones identified previously described (p56Lck) and several unreported CD4-interacting proteins, including a fragment of the MyoD family inhibitor (BC007836), the I-mfa domain-containing protein (HIC; AY196485), homeodomain-interacting protein kinase 2 (HIPK2; NM_022740), and two independent isolates of the actin-binding protein filamin-A (NM_001456). Interaction specificity was verified by one-on-one transformation, as $CD4^{IC}$ cotransfection with MyoD, HIC, HIPK2 or filamin-A permitted transformed colonies to grow in medium lacking adenosine, histidine, tryptophan and leucine, and to turn blue in a β-galactosidase assay (Fig. 1a). Of these CD4-binding proteins, we focused on filamin-A, which binds to a number of membrane receptors and signal transduction intermediates, including some regulatory cofactors of the Rho GTPases family[8,9].

Filamin-A consists of two subunits with relative molecular weights (M_r) of 280K, each containing 24 immunoglobulin-like β-sheet tandem repeats of approximately 96 amino acids. The filamin-A actin-binding domain is in the amino terminus, whereas the dimerization domain is located in repeat 24 in the carboxyl terminus[10]. The shortest *filamin-A* cDNA rescued in the two-hybrid screening encoded amino acids 968–1252 and corresponded to repeats 8–10. To examine the CD4–filamin-A interaction, glutathione S-transferase (GST)-fused $CD4^{IC}$ binding to *in vitro*-translated filamin-A repeats 8–10 was examined. GST–$CD4^{IC}$, but not GST alone, interacted with the biotinylated filamin-A repeat 8–10 fragment (Fig. 1b). GST–$CD4^{IC}$ also interacted efficiently with full-length filamin-A Jurkat cell total lysates (Fig. 1c).

The filamin-A–CD4 interaction was analysed in cells using anti-CD4 antibody-coated magnetic beads for affinity immunoisolation of CD4-containing membranes obtained by nitrogen cavitation. Even in unstimulated Jurkat cells, a fraction of p56Lck and filamin-A coisolated with CD4 beads; CD4 ligation notably increased filamin-A copurification with CD4 and p56Lck (Fig. 1d). In some experiments, filamin-A was dectected as a 280K and 250K doublet; the 250K band was identified as a proteolysed form of filamin-A by mass spectrometry (data not shown). The kinetics of filamin-A interaction was further analysed with CD4 after antibody-induced CD4 activation. Before activation, a fraction of filamin-A bound to CD4; CD4 activation increased filamin-A

[1]Department of Immunology and Oncology Centro Nacional de Biotecnología, Consejo Superior de Investigaciones Científicas (CSIC), Darwin 3, Campus de Cantoblanco, 28049 Madrid, Spain. [2]Bioinformatics Unit, Centro Nacional de Biotecnología, Consejo Superior de Investigaciones Científicas (CSIC), Darwin 3, Campus de Cantoblanco, 28049 Madrid, Spain. [3]Servicio de Microbiología, Hospital 12 de Octubre, Avda. de Córdoba, 28041 Madrid, Spain. [4]CCR Nanobiology Program, National Cancer Institute-Frederick, National Institutes of Health, Frederick, MD 21702-1201, USA. [5]Venetian Institute of Molecular Medicine, University of Padova, 35100 Padua, Italy. [6]Current address: Computational and Structural Biology Group, Centro Nacional de Investigaciones Oncológicas, Melchor Fernández Almagro 3, 28029 Madrid, Spain.
[7]Correspondence should be addressed to S.M. (e-mail: smanes@cnb.uam.es)

Received 13 March 2007; accepted 29 May 2007; published online 17 June 2007; DOI: 10.1038/ncb1610

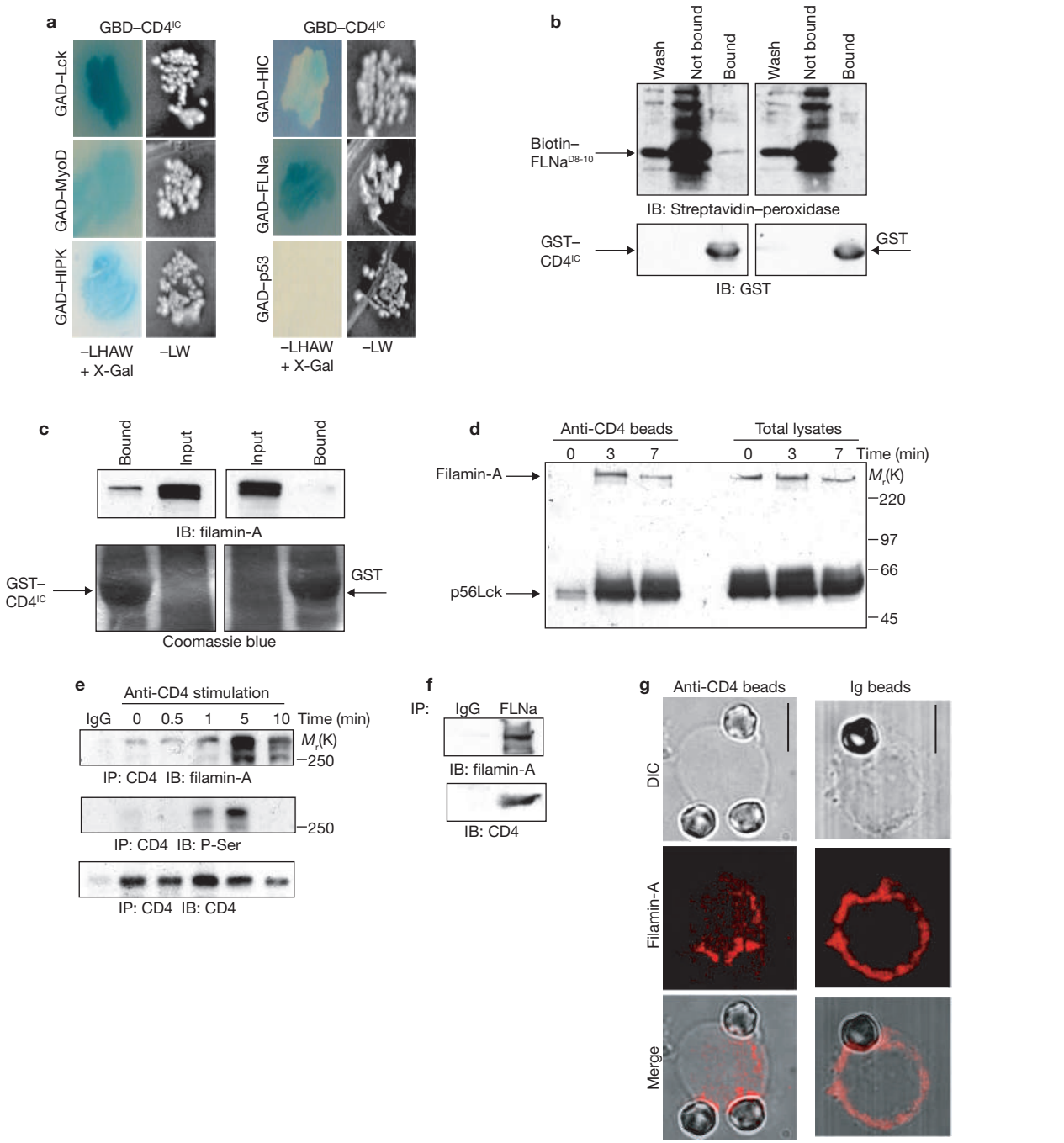

Figure 1 Identification of filamin-A as a CD4-binding protein. (**a**) Growth and β-galactosidase activity of yeast colonies cotransfected with the indicated plasmids on –LW and –LHAW selection plates after 72 h; blue indicates specific interaction of the two proteins. FLNa, filamin-A. (**b**) Pulldown of *in vitro*-translated, biotin-labelled filamin-A (residues 968–1252) interaction with GST–CD4^{IC} or GST, analysed by immunoblot. A fraction of the non-retained material (not bound), the first wash step and eluted proteins (bound) are shown. (**c**) GST or GST–CD4^{IC} were incubated with total cell extracts and pulldown performed. Immunoblot of GST-bound proteins and cell extracts (input) using anti-filamin-A antibody (top) and Coomassie blue staining of the gel (bottom). (**d**) Immunoisolation of CD4 with anti-CD4-coated magnetic beads after nitrogen cavitation of cells. Affinity-isolated membranes (left) and cell lysates (right) were blotted with indicated antibodies. (**e**) MT-2 cells were incubated with an activating anti-CD4 antibody, immunoprecipitated with anti-CD4 or IgG and SDS–PAGE-resolved CD4-bound proteins were blotted sequentially with the indicated antibodies. (**f**) Membrane proteins immunoprecipitated (IP) with control IgG or anti-filamin-A antibodies were blotted for CD4 and filamin-A. (**g**) Coredistribution of endogenous CD4 and filamin-A. Jurkat cells were incubated with IgG- or anti-CD4-coated beads, fixed and stained with anti-filamin-A antibody (red). Merge of transmission and red fluorescence images is shown. Representative cells are shown from more than 30 cells recorded in two experiments. The scale bars represent 10 μm.

association, with a peak at 5 min (Fig. 1e). β-Actin was not detected in anti-CD4 immunoprecipitates (see Supplementary Information, Fig. S1a), suggesting that coprecipitation of filamin-A with CD4 is not the consequence of non-specific cosedimentation with the actin cytoskeleton during immunoprecipitation. Notably, antibody-induced CD4 activation caused filamin-A phosphorylation on serine (Fig. 1e),

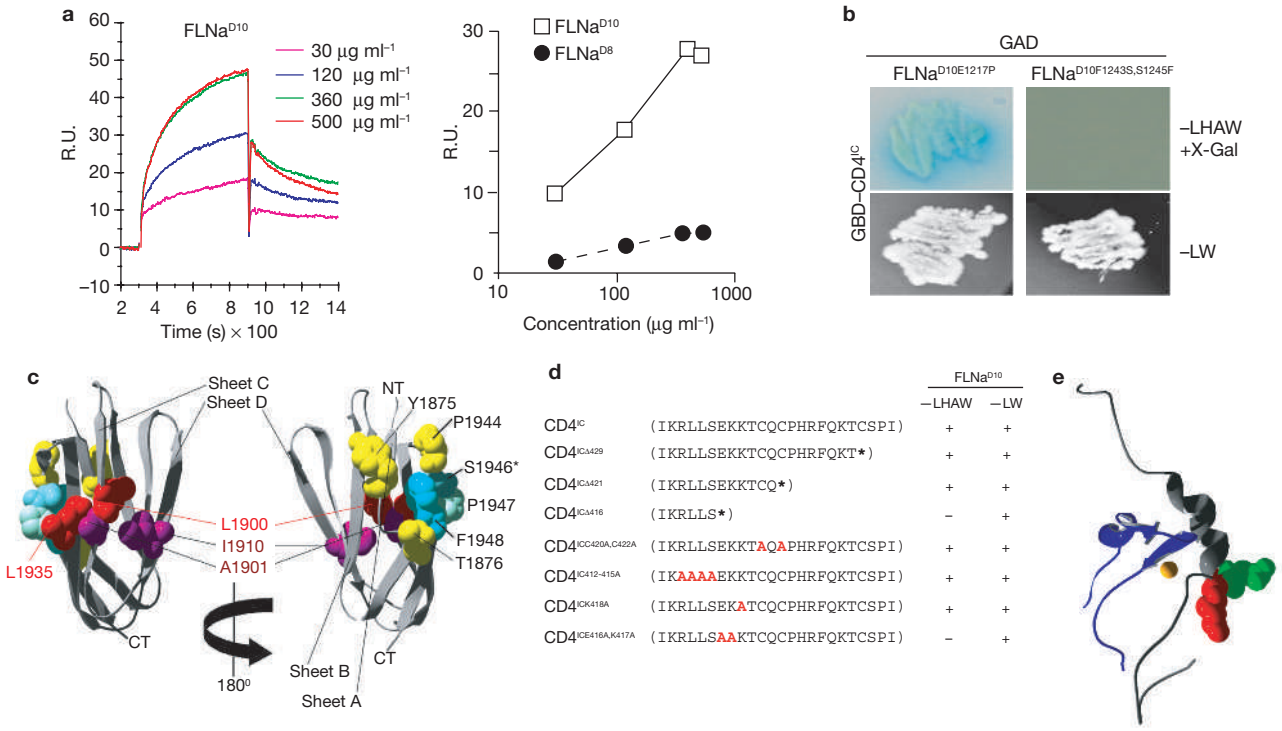

Figure 2 Identification of residues involved in the filamin-A–CD4 interaction. (**a**) Analysis of the interaction of purified GST–filamin-A repeat 10 to immobilized GST–CD4^{IC} by surface plasmon resonance. The left panel shows representative sensograms obtained with different concentrations of GST–filamin-A repeat 10 after subtracting the signal to immobilized BSA; the right panel shows response unit (RU) values obtained 30 s post-injection for GST–repeat 10 and GST–repeat 8 bound to immobilized GST–CD4^{IC}, after subtracting signals for immobilized GST ($n = 2$). (**b**) Yeast two-hybrid analysis of the interaction of filamin-A repeat 10 point mutants with CD4^{IC}. Colony growth and blue staining confirmed positive interactions. (**c**) Prediction of binding regions. Filamin-A repeat 17 was used as a master structure to predict binding patches in the multiple sequence alignment of the 24 filamin repeats (see Methods). Binding interface built by β-sheets C and D (left); the predicted binding region built by β-sheets A and B (right; rotation 180° over the *z*-axis). Residues predicted to be involved in binding and those involved in CD4 binding are shown as space-fill. Residue numbering follows PDB numbering for chain A of repeat 17. Colours indicate the degree of prediction reliability: red is the highest, followed by purple and less reliable predictions are in yellow. Cyan indicates residues involved in CD4 binding; filamin-A Phe 1948 (repeat 17) was detected with high reliability, but is shown in cyan due to its involvement in CD4 interaction. Asterisks mark residues swapped in repeat 10 (filamin-A Ser 1946 and Phe 1948 in repeat 17 corresponds to Phe 1243 and Ser 1245 in repeat 10, respectively). (**d**) Summary of results from analysis of CD4^{IC} mutant interaction with filamin-A repeat 10 by the yeast two-hybrid system. Asterisks indicate termination of the protein; single amino acid substitutions are shown in red. + indicates colony growth and – no growth; all colonies that grew in selective –LHAW medium were positive for β-galactosidase activity. (**e**) Structure of CD4 and p56Lck fragments. CD4 is shown in grey and p56Lck in blue; the yellow ball is the Zn^{2+} molecule that links the two proteins. CD4 residues involved in filamin-A interaction are shown as space-fill in green (Glu 416) and red (Lys 417).

but not on tyrosine residues (data not shown), although filamin-A is reported to be a p56Lck substrate *in vitro*[11]. In addition, CD4 coprecipitated with filamin-A (Fig. 1f). Finally, endogenous filamin-A and CD4 distribution was analysed in Jurkat cells incubated with anti-CD4-coated beads. In 98% of cell–bead conjugates, filamin-A staining accumulated at the contact interface between the CD4-expressing cell and the bead (Fig. 1g).

To further refine the filamin-A–CD4 interaction, the ability of filamin-A deletion mutants to interact with CD4^{IC} was examined by two-hybrid analysis, and repeat 10 (residues 1158–1252) was identified as the minimum CD4^{IC}-interaction domain (data not shown). In surface plasmon resonance assays, affinity purified GST–filamin-A repeat 10, but not repeat 8, interacted with GST–CD4^{IC} in a dose-dependent manner (Fig. 2a). In Jurkat cells, the filamin-A repeat 10–12 fragment bound specifically to CD4; this fragment reduced CD4 interaction with endogenous filamin-A by 55% (see Supplementary Information, Fig. S1a). HIV–gp120 also induced CD4 clustering and colocalization with the GFP–filamin-A repeat 10 fragment (see Supplementary Information, Fig. S1b). These data suggest that filamin-A repeat 10 interacts with CD4 *in vitro* and in live cells.

Sequence analysis of the 24 filamin-A repeats using structural information from the filamin-A repeat 17–GPIbα complex[12] identified three residues (Glu 1217, Phe 1243 and Ser 1245) in repeat 10 that differ from the remaining sequences in the overall alignment (see Supplementary Information, Fig. S1c). Replacement of Glu 1217 with proline (filamin-A$^{D10(E1217P)}$) did not affect the filamin-A–CD4 interaction (Fig. 2b). The specific arrangement of repeat 10 residues Phe 1243 and Ser 1245 (Ph e 1243Pro 1244Ser 1245) differs from the classical Ser–Pro–Phe motif found in the other repeats. A repeat 10 swap mutant, in which Phe 1243 and Ser 1245 were interchanged to yield the Ser–Pro–Phe arrangement (filamin-A$^{D10(F1243S,S1245F)}$), lost CD4^{IC} interaction (Fig. 2b).

To estimate interaction surfaces[13], repeat 10 was modelled using the structure of filamin-A repeat 17. Two main interfaces were predicted with high reliability as important for binding to partners. One involved β-sheets C and D, which interact with GPIbα and the β7 integrin tail[12,14]; this is considered a general binding interface[14]. The second interface involved β-sheets A and B, which include the Phe 1243Pro 1244Ser 1245 residues predicted to interact with CD4 (Fig. 2c); the prediction of this second interaction surface supports filamin-A–CD4 binding. Nevertheless, we cannot distinguish whether CD4

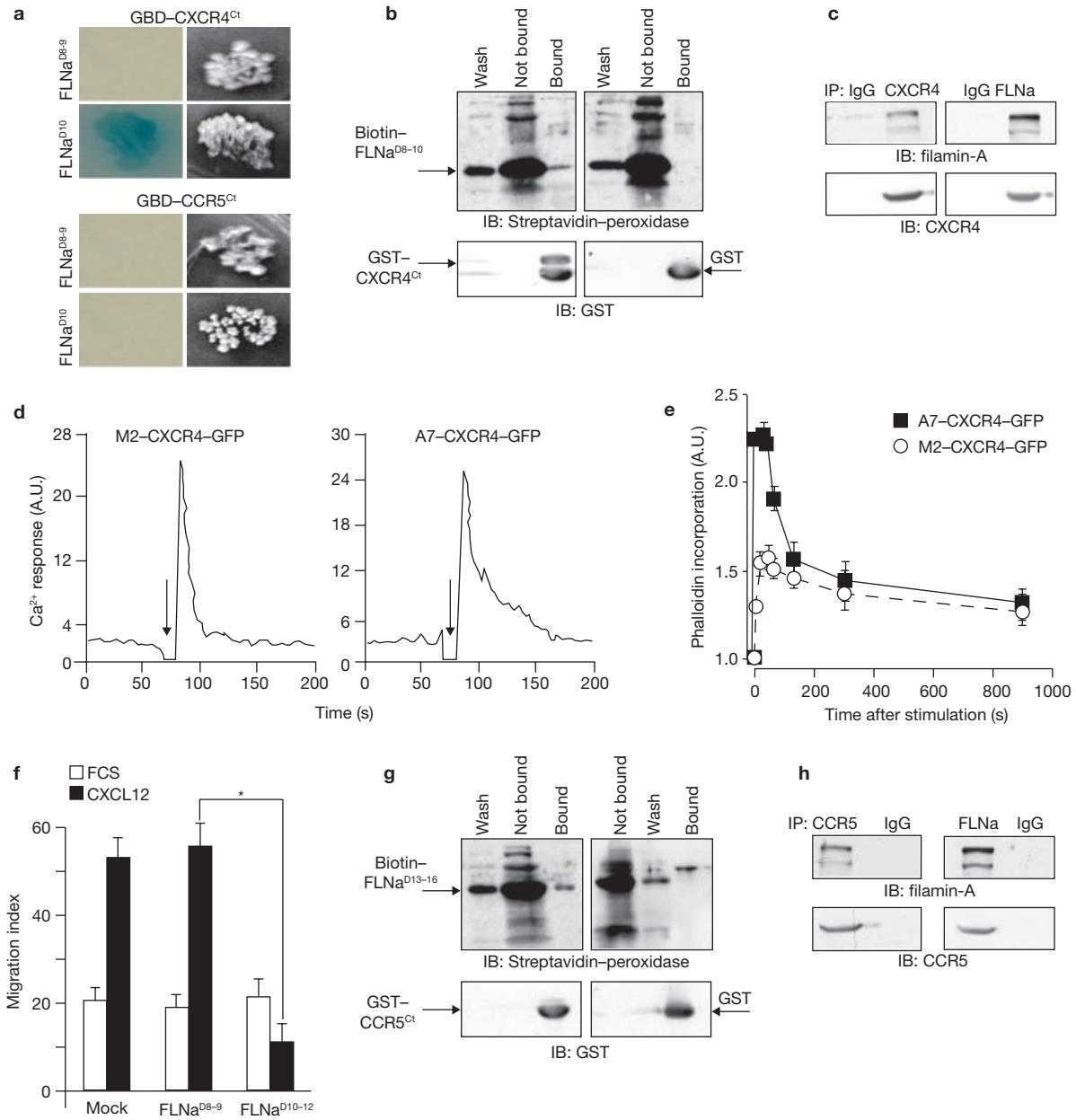

Figure 3 Filamin-A interaction with CXCR4 and CCR5. (**a**) Yeast cells were cotransfected with GAD–FLNa^{D8-9} or GAD–FLNa^{D10} plus GBD–CXCR4$^{314-360}$. Cotransformants were selected and colonies assayed as in Fig. 1a. (**b**) The interaction between *in vitro*-translated, biotin-labelled filamin-A (residues 968–1252) with GST–CXCR4^{Ct} or GST was analysed as in Fig. 1b. (**c**) Equal amounts of membrane extracts were immunoprecipitated with control IgG, anti-CXCR4 or -filamin-A, and immunoblotted with specific antibodies. (**d**, **e**) M2–CXCR4–GFP and A7–CXCR4–GFP cells were assayed for CXCL12-induced Ca^{2+} mobilization (**d**) with the Fluo-3,AM probe, or F-actin formation (**e**) measured as phalloidin incorporation. For Ca^{2+} mobilization, a representative histogram is shown; for F-actin formation, the error bars represent the mean ± s.e.m. of triplicates (n = 3). Arrow in **d** indicates agonist stimulation. (**f**) Jurkat cells transfected with indicated filamin-A fragments were assayed for chemotaxis towards CXCL12 or FCS (10%) in transwell assays. Migration index was calculated by dividing the number of cells that migrated in response to the agonist by the number of cells that migrated in response to medium alone for each condition. The error bars represent the mean ± s.e.m. (n = 3; the asterisk indicates P <0.001, two-tailed Student's t-test). (**g**) Interaction of *in vitro*-translated, biotin-labelled filamin-A repeats 13–16 with GST–CCR5^{Ct} or GST was analysed by pulldown, as in Fig. 1b. (**h**) Equal amounts of membrane extracts were immunoprecipitated with control IgG, anti-CCR5, or -filamin-A, and immunoblotted with indicated antibodies.

interacts directly with Phe–Pro–Ser residues or whether the Phe–Pro–Ser arrangement induces a conformational change that exposes other binding interfaces in repeat 10, enabling CD4 interaction. Moreover, three-dimensional modelling indicates that the unique Phe–Pro–Ser arrangement in repeat 10 might induce major local reorganization of this region, rendering this repeat substantially different from other filamin-A repeats.

To locate the CD4 region responsible for filamin-A interaction, mutagenesis and sequence analysis was combined (Fig. 2d). One-on-one transformation analysis of the interaction of three CD4^{IC} deletion mutants (CD4$^{IC\Delta429}$, CD4$^{IC\Delta421}$ and CD4$^{IC\Delta416}$) with filamin-A repeat 10 identified the filamin-A binding site within CD4 residues 415–421, near the dileucine motif involved in CD4 endocytosis[15]. This region, as well

as the high-affinity binding CxCP motif, has been implicated in CD4 interaction with p56Lck[16]. Mutation of the CxCP motif abolished $CD4^{IC}$ interaction with p56Lck, but not with filamin-A (Fig. 2d). Filamin-A also coisolated with p56Lck after CD4 engagement (Fig. 1d), suggesting simultaneous CD4 interaction with p56Lck and filamin-A. Based on the available three-dimensional structure of the p56Lck–CD4 complex (PDB code 1Q68), the CD4 residues that bind p56Lck were eliminated. This allowed identification of Glu 416 and Lys 417 at the α-helix turn, predicted by n-capping to be critical for CD4 interaction with filamin-A (Fig. 2e). Furthermore, mutation of Glu 416 and Lys 417 ($CD4^{ICE416A,K417A}$) abolished CD4–filamin-A interaction, whereas alanine replacement of residues 412–415 ($CD4^{IC412–415A}$) or Lys 418 ($CD4^{ICK418A}$) did not affect filamin-A binding (Fig. 2d). These results suggested Glu 416 and Lys 417 as critical CD4 residues for interaction with filamin-A.

A small motif with a charge similar to that of CD4 was identified in CXCR4 (see Supplementary Information, Fig. S2a). As predicted by sequence analysis, two-hybrid screening showed that filamin-A repeat 10 interacted with the last intracellular loop of CXCR4 ($CXCR4^{Ct}$; amino acids 307–353), but not with the C-terminus of CCR5 ($CCR5^{Ct}$; amino acids 325–352), a receptor lacking this motif (Fig. 3a). $CXCR4^{Ct}$ fused to GST, but not GST alone, interacted with the *in vitro*-translated biotinylated filamin-A repeat 8–10 fragment (Fig. 3b). Endogenous filamin-A also coprecipitated with CXCR4 and *vice versa* (Fig. 3c); no β-actin was detected in these immunoprecipitates (see Supplementary Information, Fig. S2b). Finally, the filamin-A repeat 10–12 fragment bound to and reduced CXCR4 interaction with endogenous filamin-A by 37% (see Supplementary Information, Fig. S2b).

To determine the influence of filamin-A on CXCR4 function, we analyzed CXCR4 signalling induced by its ligand, CXCL12, in the C-terminal GFP-tagged CXCR4-transfected cell lines M2 (filamin-A-deficient) and A7 (a filamin-A-expressing M2 clone). CXCL12-induced Ca^{2+} flux, a G protein-mediated event, was comparable in M2–CXCR4–GFP and A7–CXCR4–GFP cells (Fig. 3d). In contrast, CXCL12-induced F-actin formation was impaired in filamin-A-deficient M2–CXCR4–GFP cells (Fig. 3e). Specific blockade of CXCR4–filamin-A interaction by overexpressing the filamin-A repeat 10–12 fragment inhibited CXCL12-induced chemotaxis in Jurkat cells; this fragment did not affect chemotaxis towards foetal calf serum (Fig. 3f).

Although the $CCR5^{Ct}$ did not interact with repeat 10, the two-hybrid system was used to screen its interaction with filamin-A fragments covering repeat 8 to repeat 24. $CCR5^{Ct}$ interacted with the filamin-A fragment containing repeats 13–16 (data not shown). We also observed the GST–$CCR5^{Ct}$ interaction with the *in vitro*-translated filamin-A repeat 13–16 fragment (Fig. 3g); endogenous filamin-A and CCR5 also coprecipitated in cells (Fig. 3h). As for CXCR4, filamin-A expression did not affect CCR5-mediated Ca^{2+} flux, but regulated F-actin remodelling (data not shown). These results suggest that filamin-A modulates specific CXCR4- and CCR5-mediated signalling pathways.

We next explored filamin-A function in the initial steps of HIV-1 entry into cells. HIV-1 infection is an actin- and cholesterol-dependent process in cells with physiological CD4 and coreceptor levels[7]; coreceptor overexpression abolishes these requirements[17]. Filamin-A function was examined in Env-induced cell–cell fusion by knocking down filamin-A expression with small interfering RNA (siRNA) in HEK-293-CD4 target cells, which express endogenous CXCR4 and physiological CD4 levels[18]. HEK-293 cells transiently transfected with the CXCR4-tropic env_{IIIB}, envelope were used as effectors. *Filamin-A* siRNA reduced Env-induced fusion by ~50% at 48 h post-transfection, compared to non-specific siRNA-transfected cells (Fig. 4a). At 48 h post-transfection, specific siRNA-induced knockdown of filamin-A expression also diminished cell infection by a replication-defective HIV-1 variant pseudotyped with NL4.3 (CXCR4-tropic; Fig. 4b) or ADA envelopes (CCR5-tropic; Fig. 4c). Transfection of *filamin-A* siRNA-expressing cells with full-length *filamin-A* cDNA partially rescued virus infectivity in both cases (Fig. 4b, c). Cell infection with VSV-G-pseudotyped viruses was comparable in all conditions. In an attempt to induce stable knockdown of the protein, lentiviral vectors expressing *filamin-A* short hairpin RNA (shRNA) were generated. After 72 h, lentiviral delivery of a *filamin-A*-specific shRNA vector reduced infection by NL4.3 and ADA particles, although there was slight recovery in cell infection at 96 h, probably due to the toxic effect of this shRNA (Fig. 4d). We nonetheless found that NL4.3- and ADA-pseudotyped viruses efficiently infected filamin-A-deficient M2 cells that overexpressed CD4 and CXCR4 or CCR5 (data not shown). These results do not eliminate a possible role for filamin-A in virus infection, given the high receptor and coreceptor levels expressed in these cells and/or hypothetical compensation by other filamin isoforms.

Given the large number of filamin-A binding partners, the effect observed in RNA interference (RNAi) experiments could be independent of filamin-A interaction with HIV receptors. Therefore, infection of target cells overexpressing the filamin-A repeat 10–12 fragment, which specifically hinders filamin-A interaction with CD4 and CXCR4, was analysed. Overexpression of this fragment decreased cell infection by CXCR4-tropic-pseudotyped HIV-1 viruses by ~40% (Fig. 4e). Filamin-A repeats 10–12, but not repeats 8–9 or the swap mutant repeat $10^{(F1243S,S1245F)}$ fragments, also diminished Env-induced fusion between HEK-293 CD4 and Env-expressing cells (Fig. 4f).

HIV-1 infection might require actin-dependent virus receptor clustering in the target cell[6,19]. Crosslinking was used to study the effect of filamin-A expression on CD4 mobility in M2–CD4 and A7–CD4 cell lines and both expressed comparable CD4 levels (see Supplementary Information, Fig. S3a). CD4 clustering at 37 °C was greatly reduced in M2–CD4 compared to A7–CD4 cells (see Supplementary Information, Fig. S3b). In M2–CD4 cells, CD4 was distributed in small clusters with an average area of $0.32 \pm 0.06\ \mu m^2$, whereas cluster size in A7–CD4 cells averaged $1.125 \pm 0.22\ \mu m^2$. The size range of CD4 clusters also differed significantly between M2 and A7 cells ($\chi^2 = 27.5$, $P = 0.001$, four degrees of freedom; see Supplementary Information, Fig. S3c). When antibody-induced crosslinking was performed at 12 °C, a temperature that abrogates cell metabolism, CD4 cluster size was comparable in M2 and A7 cells (mean areas $0.146 \pm 0.02\ \mu m^2$ and $0.155 \pm 0.022\ \mu m^2$, respectively; see Supplementary Information, Fig. S3d, e).

To determine the role of filamin-A in Env-induced receptor clustering, conjugates were formed between Env_{IIIB}-expressing HEK-293 cells and stable M2–CD4–CXCR4–GFP or A7–CD4–CXCR4–GFP target cells. CXCR4–GFP expression in 100% of target cells allowed their discrimination from effector cells. CXCR4–GFP accumulation at the effector:target cell interface was not observed in filamin-A-deficient cells; CXCR4 redistribution paralleled filamin-A (Fig. 4g and see Supplementary Information, Fig. S3f) and actin (see Supplementary Information, Fig. S3g) concentration at the contact site. CXCR4–GFP, filamin-A and actin did not redistribute in conjugates formed with CD4-negative A7–CXCR4–GFP cells.

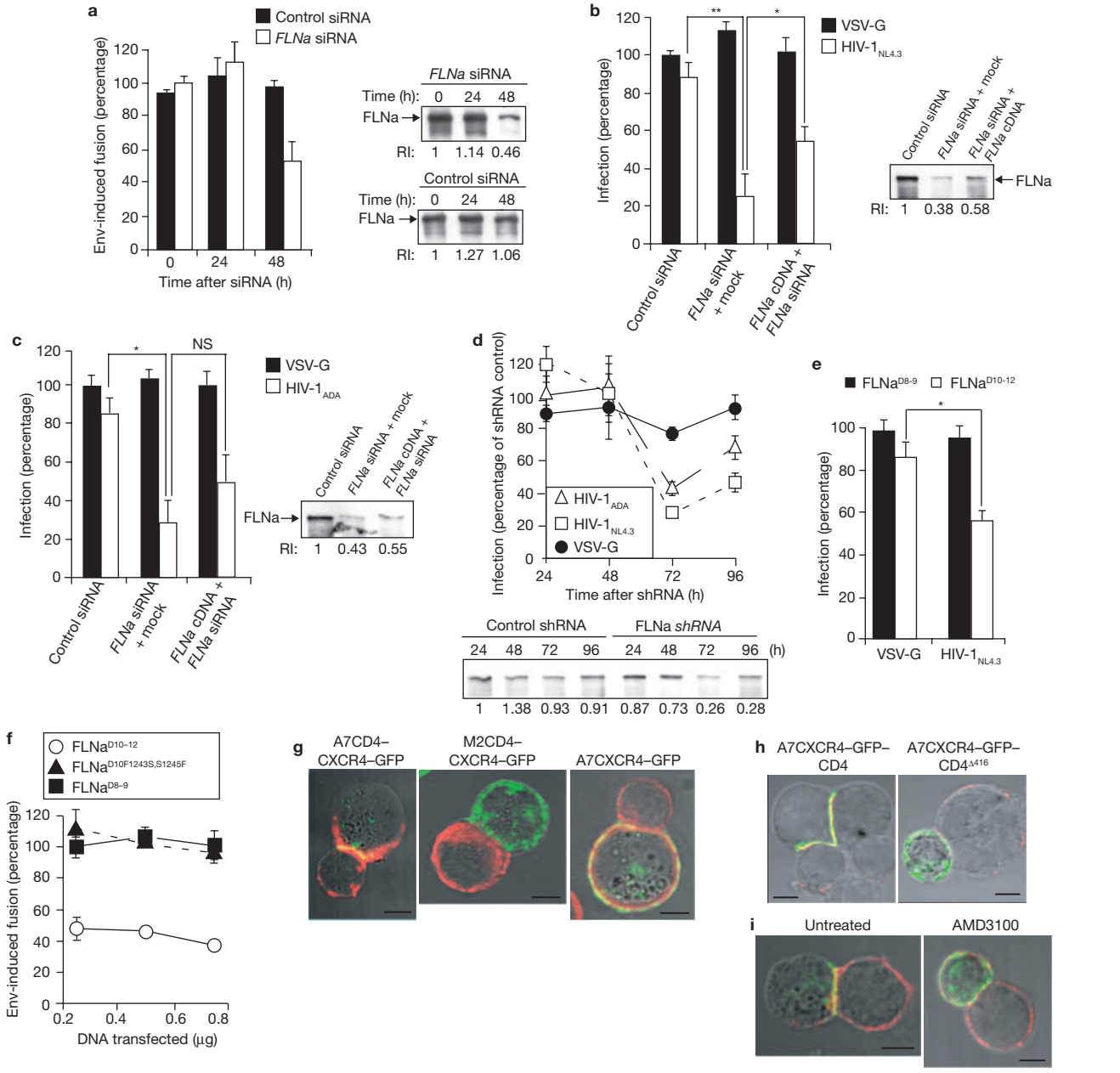

Figure 4 Filamin-A involvement in HIV-1 receptor clustering and cell infection. (**a**) Cell–cell fusion between HEK-293 Env_{IIIb} effector cells and HEK-293 CD4 target cells transfected with control or *filamin-A* siRNA, at indicated times post-transfection. Data are expressed as the percentage of Env-induced fusion, using mock-transfected cells as reference value. The immunoblot shows the filamin-A knockdown obtained at each time point. The relative filamin-A reduction index (RI) was calculated as the quotient of the densitometry signal for the filamin-A band and that for transferrin receptor (data not shown), and then normalized by the ratio obtained at time 0 (considered 1). (**b**, **c**) Infection of cells transfected with control or *filamin-A* siRNA and retransfected 24 h later with full-length *filamin-A* cDNA or empty vector (mock), using a replication-deficient NL4.3 variant pseudotyped with VSV-G, CXCR4-tropic (**b**) or CCR5-tropic (**c**) HIV-1. Immunoblots show filamin-A knockdown in each condition. Data are expressed as percentage of infection using mock-transfected cells as 100% ($n = 5$). (**d**) Cells were infected with lentivirus encoding shRNA specific for *filamin-A* or empty vector (shRNA control), and infected at indicated times as above. The immunoblot shows the FLNa knockdown at each time point. (**e**) Jurkat cells stably expressing repeats 10–12 ($FLNa^{D10–12}$) or repeats 8–9 ($FLNa^{D8–9}$) were infected with VSV-G- or CXCR4-tropic-pseudotyped HIV-1 ($n = 3$). (**f**) Cell–cell fusion between HEK-293 Env_{IIIb} cells and HEK-293 CD4 target cells transfected with mock, $FLNa^{D10–12}$, $FLNa^{D8–9}$ or $FLNa^{D10F1243S,S1245F}$ swap mutants ($n = 3$). The error bars in **a**–**f** represent the mean ± s.e.m. of triplicates in one representative experiment (the double asterisk indicates $P < 0.005$, the single asterisk indicates $P < 0.05$, NS, not significant; two-tailed Student's *t*-test). (**g**) A7–CD4–CXCR4–GFP, M2–CD4–CXCR4–GFP or A7–CXCR4–GFP target cells were mixed with HEK-293 Env_{IIIb} effectors. Red, anti-filamin-A antibody; green, CXCR4–GFP. (**h**) A7–CXCR4–GFP cells were transiently transfected with wild-type CD4 or the $CD4^{Δ416}$ mutant, then mixed with HEK-293 Env_{IIIb} cells. Red, scFv-m9 antibody; green, CXCR4–GFP. (**i**) Conjugates formed between HEK-293 Env_{IIIb} and untreated- or AMD3100-treated CD4–YFP-expressing HEK-293 cells. Red, anti-filamin-A antibody; green, CD4-YFP. The images in **g**–**i** are representative of at least 20 cells in two independent experiments and the scale bars represent 10 μm. Single colour images are shown in the Supplementary Information.

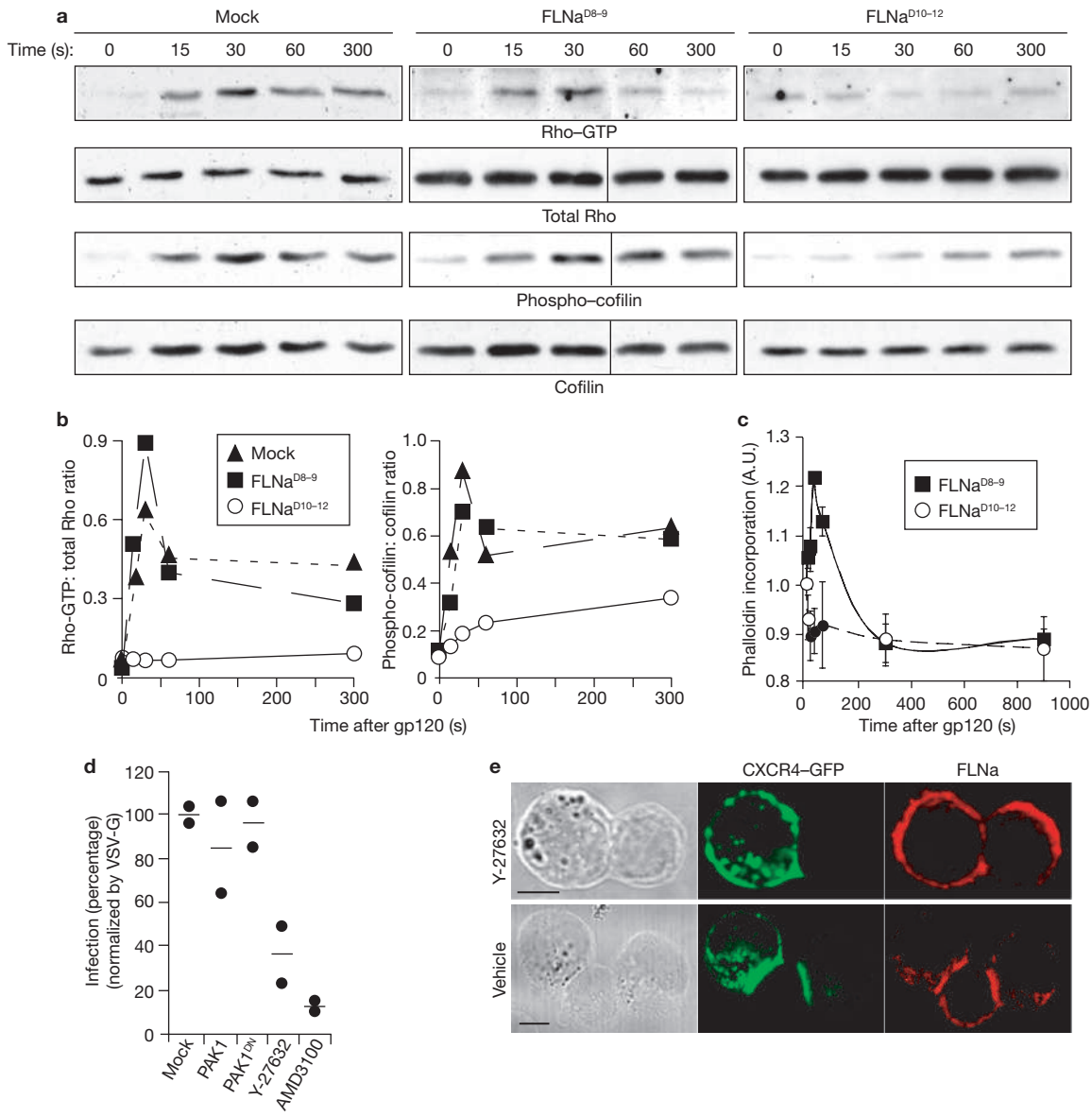

Figure 5 Filamin-A involvement in gp120-induced signalling. (**a**, **b**) Mock-, FLNa^{D10-12}- or FLNa^{D8-9}-transfected HEK-293 CD4 cells were incubated with gp120$_{IIIB}$-coated beads. Equal amounts of cell extracts were RBD-precipitated and/or blotted with indicated antibodies. Quantification of relative Rho–GTP and phospho–cofilin levels is shown in **b**; each data point represents average densitometry values ($n = 2$). (**c**) Cells as in **a** were analysed for F-actin formation by measuring phalloidin incorporation. The error bars represent the mean ± s.e.m. ($n = 3$). (**d**) HEK-293 CD4 cells were transfected with expression plasmids or treated with ROCK inhibitor Y-27632 or CXCR4 antagonist AMD-3100 (control). The percentage of infection was calculated using untransfected or DMSO-treated cells (for Y-27632 treatment) as references. The mean and actual data points are shown ($n = 2$). (**e**) Conjugates were formed between effector and vehicle- or Y-27632-pretreated filamin-A-expressing A7–CD4–CXCR4–GFP target cells. Red, anti-filamin-A antibody (red); green, CXCR4–GFP. Representative cells are shown ($n = 35$). The scale bars represent 10 μm

Similarly, the CCR5-tropic envelope also induced filamin-A-dependent CCR5 and actin accumulation at the HEK-293 *Env*$_{ADA}$:A7–CD4–GFP–CCR5 cell interface (see Supplementary Information, Fig. S3h).

It was suggested that CD4 engagement is sufficient to trigger dynamic reorganization of chemokine receptors and F-actin[20]. We formed conjugates using A7–CXCR4–GFP cells transiently transfected with wild-type CD4 or the CD4$^{\Delta 416}$ mutant, which does not interact with filamin-A. To visualize gp120 complexed with clustered CD4 we used m9, a single-chain (sc)Fv derived from an anti-gp120 Fab (X5) with higher binding affinity for CD4–gp120 complexes than for gp120 alone[21]. CXCR4–GFP and scFv–m9 staining concentrated at the interface between effector and wild-type CD4-expressing target cells, whereas these markers showed diffuse staining in CD4$^{\Delta 416}$-expressing cells (Fig. 4h and see Supplementary Information, Fig. S3i). Target-cell treatment with the CXCR4 antagonist AMD3100 prevented filamin-A, CXCR4–GFP (see Supplementary Information, Fig. S3j) and CD4 accumulation at the target:effector cell interface (Fig. 4i and see Supplementary Information, Fig. S3k), indicating that both CD4 and CXCR4 signals are necessary for filamin-A-mediated receptor clustering.

To study the mechanism by which filamin-A influences cell infection, Env-induced RhoGTPase activation was analysed in Jurkat cells transfected with distinct filamin-A fragments; CD4 and CXCR4

crosslinking was stimulated with $gp120_{IIIB}$-coated beads. Studies using viral particles indicated that HIV-1 binding induces specific RhoA activation[22]. Here, gp120 beads induced RhoA activation in mock- or filamin-A repeat 8–9-transfected Jurkat cells, whereas filamin-A repeat 10–12 fragment overexpression inhibited gp120-induced RhoA activation (Fig. 5a, b).

RhoA signals through two effectors, mDia and p160ROCK. LIM kinase (LIMK) is a ROCK target that phosphorylates and inactivates actin depolymerization factor (ADF)–cofilin, leading to F-actin stabilization[23]. gp120 binding induced rapid cofilin phosphorylation in mock- or repeat 8–9 fragment-transfected cells, with a peak 30 s after gp120 addition. Cofilin phosphorylation was severely impaired in filamin-A repeat 10–12 fragment-expressing cells, with only a slight increase after long incubation periods (Fig. 5a, b). Compatible with RhoA activation and cofilin phosphorylation-inactivation kinetics, gp120 increased F-actin levels after 30 s in cells that expressed the repeat 8–9, but not the repeat 10–12 fragment (Fig. 5c).

The LIMK–cofilin pathway can be initiated by ROCK or by the Rac effector PAK-1, and PAK-1 and ROCK both interact with filamin-A[24,25]. Treatment with the ROCK inhibitor Y-27632 inhibited Jurkat cell infection by CXCR4-tropic-pseudotyped HIV-1; in contrast, overexpression of the mutant $PAK\text{-}1^{R229,H83L,H86L}$ (PAK^{DN}, with mutations in kinase and GTPase-binding domains) did not affect virus infectivity (Fig. 5d). Expression of the dominant-negative mutant $RhoA^{N19}$ or treatment with Y-27632 also reduced Env-mediated cell–cell fusion, whereas abrogation of Rac or PAK-1 function did not (see Supplementary Information, Fig. S4a). Y-27632 prevented CXCR4, filamin-A and actin accumulation at the target:effector cell interface (Fig. 5e and see Supplementary Information, Fig. S4b), indicating that these events are ROCK-dependent. The results thus implicate filamin-A-dependent activation of the RhoA–ROCK–LIMK–cofilin pathway as a major event in gp120-induced receptor clustering. We also observed RhoA activation and cofilin phosphorylation in peripheral blood lymphocytes incubated with gp120 beads (see Supplementary Information, Fig. S4c), suggesting activation of this pathway in primary cells.

In summary, we found that filamin-A is a structural and functional adapter that organizes the F-actin rearrangements required for gp120-induced CD4 and coreceptor clustering. Structurally, filamin-A can link HIV-1 receptors to F-actin, enabling their mobility or anchorage after gp120 binding. Functionally, filamin-A allows activation of the RhoA–ROCK–LIMK–cofilin signalling cascade after gp120 binding to target cell lines and primary lymphocytes. These results confirm and extend the implication of RhoA in HIV-1 infection[22], and point to ROCK inhibitors as potential HIV-1 inhibitory drugs. In this interpretation, CD4-coreceptor clustering is prevented by inhibition of myosin light chain phosphorylation[6], another RhoA-ROCK-regulated process. Impairment of HIV-1 infection by reducing filamin-A levels or by interfering with filamin-A interaction with receptors also suggests a role for filamin-A in early phases of HIV-1 entry.

Finally, CD4, CXCR4 and CCR5 cocluster at the immune synapse formed between T cells and antigen-presenting cells; this clustering is important for T cell costimulation[26]. Filamin-A also interacts with CD28, another costimulatory receptor[27]. It is tempting to hypothesize that HIV-1 co-opts a filamin-A-based mechanism involved in T-cell activation to enter the target cell. □

METHODS

Cloning and generation of CD4 and filamin-A mutants. pSRαpuro–CD4 and pCD4–YFP were provided by G. del Real (Centro de Investigación en Sanidad Animal, Madrid, Spain) and T. J. Hope (Northwestern University, Chicago, IL), respectively. Filamin-A fragments for repeats 8–9, 10–12, 13–16, 16–20 and 20–24 were amplified by PCR (see Supplementary Information, Methods) and cloned in pEGFPN1, pcDNA3.1 or pGADT7. Myc-tagged filamin-A repeats 8–9 and 10–12 were also subcloned in the bicistronic plasmid pRV–IRESGFP. Selected amino acids of $CD4^{IC}$ or filamin-A repeat 10 were mutated using the Quick Change mutagenesis kit, with appropriate primer pairs (see Supplementary Information, Methods) and pfu Turbo DNA polymerase for PCR amplification, and verified the sequence of selected clones at the CNB core facility. CD4 and filamin-A mutants were subcloned in pGBKT7 and pGADT7, respectively, for two-hybrid screening.

Two-hybrid library screening. CD4, CXCR4 and CCR5 baits were constructed by PCR amplification of $CD4^{IC}$, $CXCR4^{Ct}$ and $CCR5^{Ct}$ with specific primers (see Supplementary Information, Methods); the product was subcloned into *Eco*RI–*Sal*I Gal4-binding domain vector (pGBKT7). $CD4^{IC}$ was used to screen a Jurkat cDNA library, which was generated by SMART cDNA Synthesis, fused to the Gal4 activation domain (pGADT7–Rec). Positive clones were isolated and sequenced, and verified by one-on-one transformation on agar plates lacking adenine, histidine, tryptophan and leucine, and using a X-α-Gal β-galactosidase assay.

Analysis of filamin-A interactions. GST pulldown assays were performed by incubating similar amounts of immobilized GST and GST–$CD4^{IC}$ proteins with Jurkat cell extracts (4 °C, 4 h). Bound proteins were eluted with 2× SDS–PAGE loading buffer. A fraction of eluted protein was analysed by immunoblot with anti-filamin-A or -CD4 intracellular domain antibody; the remainder was stained with Coomassie blue. Filamin-A fragments repeats 8–10 and repeats 13–16 cloned in pcDNA–Myc–His were *in vitro*-transcribed and translated using the TNT system, incorporating biotinylated lysine residues in the nascent proteins. A 50 µl aliquot was used for each GST pulldown assay, following the manufacturer's protocols. Eluted proteins were analysed by immunoblot with anti-GST or streptavidin peroxidase.

Surface plasmon resonance analyses were performed in a BIAcore 3000 (GE Healthcare, Uppsala, Sweden) apparatus. GST–$CD4^{IC}$ and GST purified on GSTrap FF columns (Amersham Biosciences, Little Chalfont, UK) were immobilized (30 µg ml^{-1} in 10 mM NaAc buffer at pH 5.0) on a CM5 sensor chip using the BIAcore Amine Coupling Kit (flow rate 5 µl min^{-1}, 7 min). A third flow cell was coated with BSA as control. After blocking unreacted sites with ethanolamine, the final response units (RU) obtained were 8226 RU, 6088 RU and 9402 RU for GST–$CD4^{IC}$, GST and BSA, respectively. Different concentrations of affinity purified GST–filamin-A repeat 10, GST–repeat 8 and GST were run over the three flow cells at 5 or 10 µl min^{-1} in running buffer (10 mM HEPES, 0.15 M NaCl at pH 7.4). The stabilization time between two cycles was 10 min.

For antibody-induced CD4 activation, 1×10^7 serum-starved cells were incubated (20 min, 4 °C) with anti-CD4 (HP2.6); goat anti-mouse Ig antibody was added and tubes incubated (37 °C) for the times indicated. The reaction was terminated by placing tubes on ice; cell pellets were washed immediately with ice-cold PBS. The membrane fraction was prepared by passing cells through 25- and 30-gauge needles in 50 mM Tris at pH 7.4, 150 mM NaCl, 5 mM EDTA and protease inhibitors, followed by centrifugation (166,000*g*, 4 °C, 1 h) on a 30–25% OptiPrep gradient. Membrane extracts (300 µg) were immunoprecipitated (3 h, 4 °C) with anti-CD4, -filamin-A or mouse IgG antibody, followed by incubation (45 min, 4 °C) with protein G–Sepharose. Precipitated proteins were analysed by immunoblot with anti-$CD4^{IC}$, -filamin-A and -phosphoserine antibody and developed with appropriate TrueBlot or secondary antibodies. For CXCR4 and CCR5 interactions, 2×10^7 Jurkat or JJCKR5–GFP cells were fractionated; membrane extracts (200 µg) were immunoprecipitated with anti-CCR5, -CXCR4, -filamin-A or control IgG antibodies, and precipitated proteins were analysed by immunoblot with indicated antibodies. Immunoisolation of plasma membrane fragments using anti-CD4 antibody is described in the Supplementary Information, Methods.

Immunofluorescence and confocal microscopy studies. To study receptor redistribution at the HIV-1 synapse, A7 and M2 cells stably expressing CD4 and CXCR4–GFP were mixed (20 min, 37 °C) with HIV-1 Env_{IIIb}-expressing HEK-293 cells. The complexes formed were fixed with 4% paraformaldehyde (PFA,

5 min, 4 °C), permeabilized with 0.1% Triton X-100 (10 min, 4 °C), and stained with anti-filamin-A, actin-rhodamine or scFv–m9, followed by appropriate secondary antibodies. In some cases, target cells were transiently transfected with actin–RFP chimera (a gift from L. Rajendran, Max-Planck-Institute of Molecular Cell Biology and Genetics, Dresden, Germany).

A7–CD4 and M2–CD4 cells were incubated (30 min, 4 °C) with anti-CD4 (HP2.6) antibody, washed and then incubated (20 min) with Cy2-anti-mouse antibody at 37 °C or 12 °C. Cells were washed with ice-cold PBS, fixed with PFA, and 10 random fields recorded for each condition in a Leica confocal imaging system with a 63× objective (NA 1.2). Images were quantified using ImageJ software. In some experiments, CD4 clustering was induced by incubation of Jurkat cells with anti-CD4-coated 4.5 μm carboxylate microspheres (1:1 ratio).

CXCR4 and CCR5 functional assays. Calcium mobilization, chemotaxis and F-actin formation assays were performed as previously described[28] (see Supplementary Information, Methods).

gp120-bead preparation. Streptavidin-coated beads (6 μm) were incubated sequentially at 4 °C with biotinylated rabbit anti-sheep IgG Fab 2 fragment, sheep-anti-gp120 antibody and recombinant $gp120_{IIIB}$ (NIH AIDS Research and Reference Reagent Program; Division of AIDS, NIAID, NIH, Bethesda, MD). PHA-activated human peripheral blood mononuclear cells (2×10^6) or Jurkat cells retrovirally transduced with mock, filamin-A repeat 10–12 or repeat 8–9 fragments (5×10^6) were stimulated with gp120 beads (ratio 2:1 for PBL, 1:1 for Jurkat). Cell extracts were analysed for active RhoA and Rac by immunoprecipitation with GST–Rhotekin and GST–PAK binding domains, respectively, or immunoblotted with anti-RhoA, -Rac, -phosphoserine, -phospo-cofilin, -cofilin or -filamin-A antibodies.

HIV-1 cell-entry assays. Cell–cell fusion assays were performed as previously described[3] (see Supplementary Information, Methods). For single-round cell infections, the lentiviral vector pNL4-3–Luc –R-E from N. Landau[29] (NIH AIDS Research and Reference Reagent Program) was used for production of VSV, X4 and R5 HIV-1 pseudotypes by transfection of VSV-G, X4 (NL4.3), or an R5 envelope (ADA or LMP0608, GenBank DQ448819) in 293T cells. Supernatants were obtained 48 h after transfection, filtered (0.45 μm pore) and frozen (–80 °C) until use. Jurkat or JJCKR5–GFP cells were infected 48 h after transfection with filamin-A-specific or control siRNA duplexes at a M.O.I of 0.1. Infectivity was measured 48 h after infection by luciferase assay.

Statistical analysis. In capping experiments, images were analysed blind to the treatment conditions. For each experimental condition, 20–30 confocal cell images were taken randomly, in at least three independent experiments. CD4 cluster-size distribution was analysed using the χ^2 test, and chemotaxis and infectivity data were compared using two-tailed Student's *t*-test. Values of *P* to determine statistical significance are indicated in the text.

Note: Supplementary Information is available on the Nature Cell Biology website.

ACKNOWLEDGEMENTS

We thank T. Stossel, D. Rodríguez, A. C. Carrera, F. Sánchez-Madrid and M. A. del Pozo for reagents and discussion, M. Martín and L. Kremer (CNB Protein Tools Unit) for BIAcore analysis, M. C. Moreno-Ortiz for cell sorting, C. M. Martínez-Garcia for technical help, and C. Mark for editorial assistance. This work was supported in part by the Spanish Ministry of Education and Science (SAF2005-00241) and the Intramural CSIC Program (PIF 20050F0212) to S.M., the European Union FP6 (INNOCHEM, LSHB-CT-2005-518167) to S.M. and C.M.A., the Instituto de Salud Carlos III (FIS030300; G030173) to R.D., and the Intramural Research Program of the NIH, National Cancer Institute, Center for Cancer Research to D.S.D. A.R. is a recipient of MIRG-CT-2005-016499. The Department of Immunology and Oncology was founded and is supported by the Spanish National Research Council (CSIC) and by Pfizer.

AUTHOR CONTRIBUTIONS

S.J.-B. designed and performed most experiments and prepared the figures. E.M. and R.A.L. obtained CD4 mutants. C.G.-M. performed functional assays and yeast two-hybrid analysis of CXCR4 and CCR5. A.R. and A. Valencia did the bioinformatic analysis. A. Viola designed the immunocavitation experiments and provided reagents. R.D. and L.M.-P designed and performed virus infection experiments. D.S.D. and C.M.-A. contributed to discussion and provided reagents. S.M. conceived the study, planned and coordinated experiments, and wrote the manuscript.

COMPETING FINANCIAL INTERESTS

The authors declare no competing financial interests.

Published online at http://www.nature.com/naturecellbiology/
Reprints and permissions information is available at http://npg.nature.com/reprintsandpermissions/

1. Dimitrov, D. Virus entry: molecular mechanisms and biomedical applications. *Nature Rev. Microbiol.* **2,** 109–122 (2004).
2. Iyengar, S., Hildreth, J. & Schwartz, D. Actin-dependent receptor colocalization required for human immunodeficiency virus entry into host cells. *J. Virol.* **72,** 5251–5255 (1998).
3. Mañes, S. *et al.* Membrane raft microdomains mediate lateral assemblies required for HIV-1 infection. *EMBO Rep.* **1,** 190–196 (2000).
4. Liao, Z., Cimakasky, L., Hampton, R., Nguyen, D. & Hildreth, J. Lipid rafts and HIV pathogenesis: Host membrane cholesterol is required for infection by HIV type 1. *AIDS Res. Human Retroviruses* **17,** 1009–1019 (2001).
5. Popik, W., Alce, T. & Au, W. Human immunodeficiency virus type 1 uses lipid raft-colocalized CD4 and chemokine receptors for productive entry into CD4(+) T cells. *J. Virol.* **76,** 4709–4722 (2002).
6. Jolly, C., Kashefi, K., Hollinshead, M. & Sattentau, Q. HIV-1 cell to cell transfer across an Env-induced, actin-dependent synapse. *J. Exp. Med.* **199,** 283– 293 (2004).
7. Mañes, S., del Real, G. & Martínez-A., C. Pathogens: raft hijackers. *Nature Rev. Immunol.* **3,** 557–568 (2003).
8. Bellanger, J. M. *et al.* The Rac1- and RhoG-specific GEF domain of Trio targets filamin to remodel cytoskeletal actin. *Nature Cell Biol.* **2,** 888–892 (2000).
9. Ohta, Y., Hartwig, J. H. & Stossel, T. P. FilGAP, a Rho- and ROCK-regulated GAP for Rac binds filamin A to control actin remodelling. *Nature Cell Biol.* **8,** 803–814 (2006).
10. Stossel, T. *et al.* Filamins as integrators of cell mechanics and signalling. *Nature Rev. Mol. Cell Biol.* **2,** 138–145 (2001).
11. Pal Sharma, C. & Goldmann, W. Phosphorylation of actin-binding protein (ABP-280; filamin) by tyrosine kinase p56lck modulates actin filament cross-linking. *Cell Biol. Int.* **28,** 935–941 (2004).
12. Nakamura, F. *et al.* The structure of the GPIb–filamin A complex. *Blood* **107,** 1925–1932 (2006).
13. Fariselli, P., Pazos, F., Valencia, A. & Casadio, R. Prediction of protein-protein interaction sites in heterocomplexes with neural networks. *Eur. J. Biochem.* **269,** 1356–1361 (2002).
14. Kiema, T. *et al.* The molecular basis of filamin binding to integrins and competition with talin. *Mol. Cell* **21,** 337–347 (2006).
15. Shin, J., Doyle, C., Yang, Z., Kappes, D. & Strominger, J. Structural features of the cytoplasmic region of CD4 required for internalization. *EMBO J.* **9,** 425–434 (1990).
16. Kim, P., Sun, Z., Blacklow, S., Wagner, G. & Eck, M. A zinc clasp structure tethers Lck to T cell coreceptors CD4 and CD8. *Science* **301,** 1725–1728 (2003).
17. Viard, M. *et al.* Role of cholesterol in human immunodeficiency virus type 1 envelope protein-mediated fusion with host cells. *J. Virol.* **76,** 11584–11595 (2002).
18. del Real, G. *et al.* Blocking of HIV-1 infection by targeting CD4 to non-raft membrane domains. *J. Exp. Med.* **196,** 293–301 (2002).
19. McDonald, D. *et al.* Recruitment of HIV and its receptors to dendritic cell–T cell junctions. *Science* **300,** 1295–1297 (2003).
20. Nguyen, D., Giri, B., Collins, G. & Taub, D. Dynamic reorganization of chemokine receptors, cholesterol, lipid rafts, and adhesion molecules to sites of CD4 engagement. *Exp. Cell Res.* **304,** 559–569 (2005).
21. Zhang, M. *et al.* Improved breadth and potency of an HIV-1-neutralizing human single-chain antibody by random mutagenesis and sequential antigen panning. *J. Mol. Biol.* **335,** 209–219 (2004).
22. del Real, G. *et al.* Statins inhibit HIV-1 infection by down-regulating Rho activity. *J. Exp. Med.* **200,** 541–547 (2004).
23. Maekawa, M. *et al.* Signaling from Rho to the actin cytoskeleton through protein kinases ROCK and LIM-kinase. *Science* **285,** 895–898 (1999).
24. Vadlamudi, R. *et al.* Filamin is essential in actin cytoskeletal assembly mediated by p21-activated kinase 1. *Nature Cell Biol.* **4,** 681–690 (2002).
25. Ueda, K., Ohta, Y. & Hosoya, H. The carboxy-terminal pleckstrin homology domain of ROCK interacts with filamin-A. *Biochem. Biophys. Res. Commun.* **301,** 886–890 (2003).
26. Molon, B. *et al.* T cell costimulation by chemokine receptors. *Nature Immunol.* **6,** 465–471 (2005).
27. Tavano, R. *et al.* CD28 interaction with filamin-A controls lipid raft accumulation at the T-cell immunological synapse. *Nature Cell Biol.* **8,** 1270–1276 (2006).
28. Gómez-Moutón, C. *et al.* Dynamic redistribution of raft domains as an organizing platform for signaling during cell chemotaxis. *J. Cell Biol.* **164,** 759–768 (2004).
29. He, J. *et al.* Human immunodeficiency virus type 1 viral protein R (Vpr) arrests cells in the G2 phase of the cell cycle by inhibiting p34cdc2 activity. *J Virol.* **69,** 6705–6711

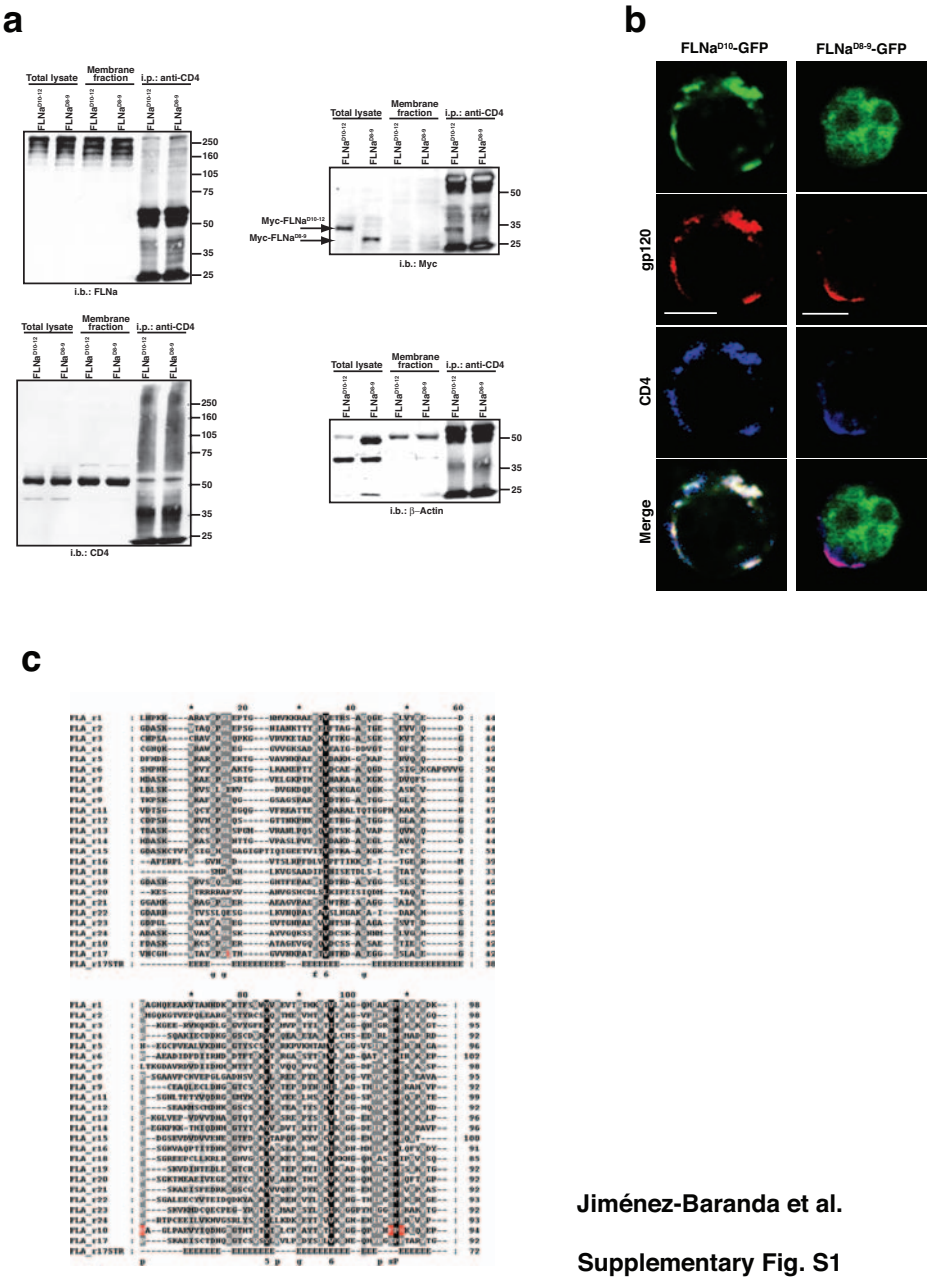

Jiménez-Baranda et al.

Supplementary Fig. S1

Figure S1. Interaction of filamin-A repeat 10 with CD4 and multiple sequence alignment of filamin-A repeats. **a,** Overexpressed filamin-A repeat 10 competes for interaction of endogenous filamin-A with CD4. Resting Jurkat cells expressing Myc-tagged filamin-A repeat 10-12 or repeat 8-9 fragments were fractionated and the membrane fraction solubilized in RIPA buffer. Membrane proteins were immunoprecipitated with anti-CD4 antibody. Proteins from anti-CD4 immunoprecipitates, the membrane fraction, and total lysates were immunoblotted sequentially with anti-filamin-A, -CD4, -Myc and β-actin antibodies. Results shown are representative of two experiments. ***b,*** gp120 induces clustering of CD4 and filamin-A repeat 10. Jurkat cells were transfected with GFP-tagged filamin-A fragments corresponding to repeats 8-9 or repeat 10, and CD4 crosslinking induced by sequential incubation with gp120 and anti-gp120 antibody (red). CD4 was stained with anti-CD4IC antibody (blue), and filamin-A fragments detected by GFP fluorescence (green) (n = 14 cells; bar = 10 μm). ***c,*** Alignment of filamin-A repeats based on published data. Amino acids in repeat 10 that differ from remaining sequences (red). Structural alignment of filamin-A repeat 17 is shown at the bottom (B, residue in isolated beta bridge; E, extended beta strand; G, 310 helix; T, hydrogen-bonded turn; S, beta strand). The leucine residue that interacts with phenylalanine is shown in red on a grey background.

a

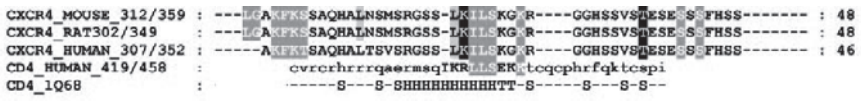

b

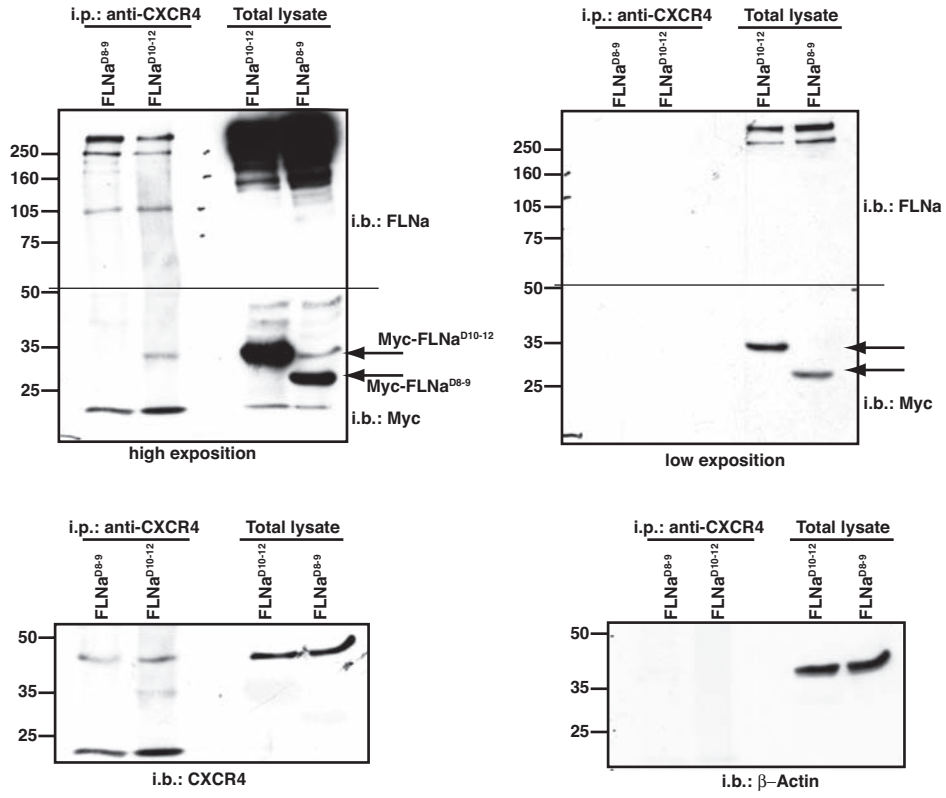

Figure S2. Interaction of filamin-A repeat 10 with CXCR4 and multiple sequence alignment of the CXCR4 C-terminus. **a,** CXCR4 C-terminal regions from various species are labelled with SwissProt numbers. The two bottom lines indicate the sequence and secondary structure of the CD4_HUMAN C-terminal tail (pdb code 1Q68). CD4 amino acids in lower case indicate regions that do not align, whereas amino acids in upper case show the motif shared by CD4 and CXCR4. CD4 residues E416 and K417, involved in filamin-A interaction, are located in a helix turn (nomenclature corresponds to 1Q68 structure; S, beta strand; H, α-helix; T, turn). ***b,*** Cells as in Supplementary Fig S1*a* were immunoprecipitated with anti-CXCR4 antibody and blotted sequentially with the indicated antibodies. The line indicates that the nitrocellulose membrane was cut and each part immunoblotted separately with anti-filamin-A or anti-Myc. Results are representative of two experiments.

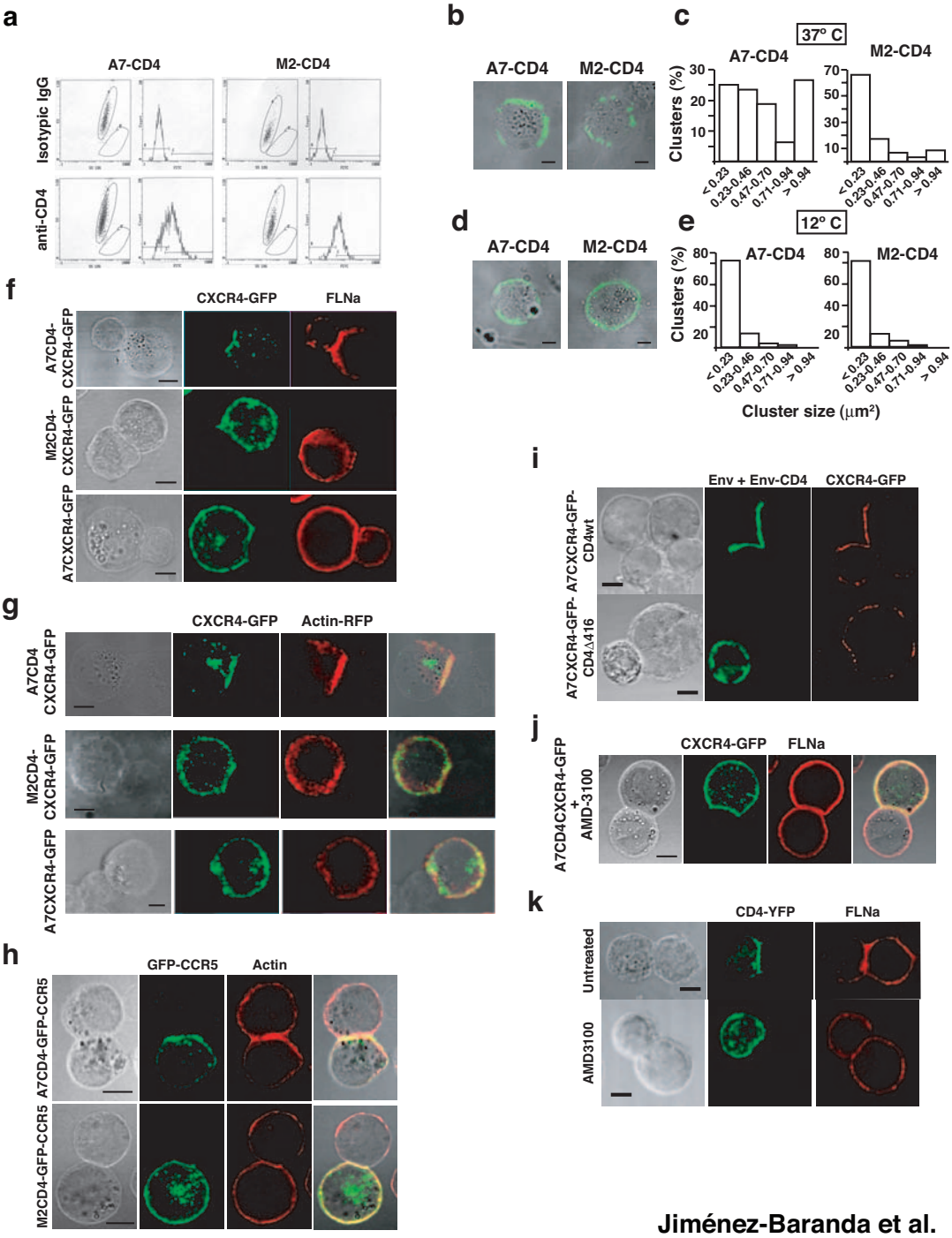

Jiménez-Baranda et al.

Supplementary Fig. S3

Figure S3. Regulation of receptor clustering by filamin-A. ***a,*** CD4 expression in stable M2-CD4 and A7-CD4 cell lines. Cells were stained with anti-CD4 or isotype-matched IgG, followed by FITC-labelled secondary antibody, and analyzed by FACS. ***b-e***, A7-CD4 and M2-CD4 cells were incubated sequentially with anti-CD4 and Cy2-anti-mouse antibody (4ºC), then transferred to 37ºC (***b***) or 12ºC (***d***) for 20 min. Cluster size was quantified (***c,e***) from cells recorded in two independent experiments (n = 85 data points from 25 A7-CD4 cells at 37ºC; n = 115 from 20 M2-CD4 cells, 37ºC; n = 64 from 19 A7-CD4 cells, 12ºC; n = 128 from 15 M2-CD4 cells, 12ºC). ***f,*** Single-colour images for Fig. 4g. ***g,*** Conjugates between HEK-293-env_{IIIb} effector cells and A7-CD4-CXCR4-GFP, M2-CD4-CXCR4-GFP, or A7-CXCR4-GFP cells transfected with red fluorescent protein (RFP)-tagged actin. Red and green staining correspond to actin and CXCR4, respectively. ***h,*** Conjugates formed between A7-CD4-GFP-CCR5 or M2-CD4-GFP-CCR5 and HEK-293-Env_{ADA} effectors. Red, phalloidin (F-actin); green, GFP-CCR5. ***i,*** Single-colour images for Fig. 4h. ***j,*** Single-colour images for Fig. 4m. ***f,*** A7-CD4-CXCR4-GFP target cells were pre-treated with the CXCR4 antagonist AMD-3100. Conjugates with *Env*-expressing effector cells were stained with anti-filamin-A antibody (red); CXCR4 (green). ***k,*** Single-colour images for Fig. 4i. Bar = 5 μm (***b,d***); 10 μm (***f-k***).

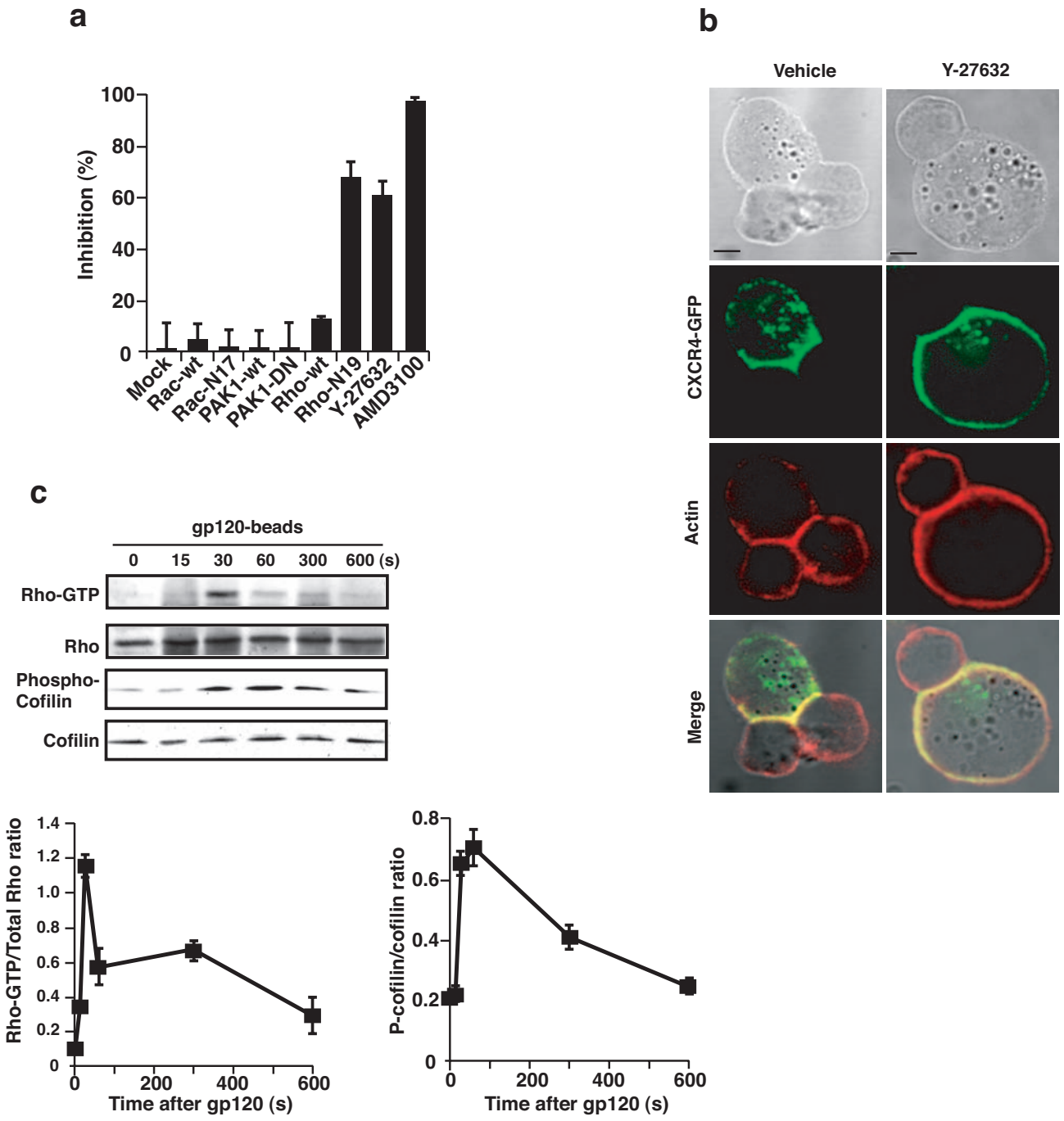

Figure S4. RhoA pathway activation in primary cells and involvement in Env-induced receptor clustering. **a,** Env-mediated cell-cell fusion. HEK-293-CD4 cells were transfected with expression plasmids, or treated with ROCK inhibitor Y-27632 or CXCR4 antagonist AMD-3100 (control). Percentage of inhibition was calculated using untransfected or DMSO-treated cells as references. Data show mean ± SEM ($n = 2$). ***b***, Conjugates between HEK-293-env_{IIIb} effector cells and vehicle- or Y-27632-treated A7-CD4-CXCR4-GFP cells. Actin (red), CXCR4 (green). Bar = 10 μm ($n = 20$). ***c***, Activated human primary lymphocytes were incubated with gp120 beads; equal amounts of cell extracts were assayed for active RhoA-GTP. Blots were performed using anti-RhoA, -phosphocofilin and -cofilin antibodies. Relative RhoA-GTP and phosphocofilin levels (bottom); each data point represents the mean ± SEM of densitometry values from two independent experiments.

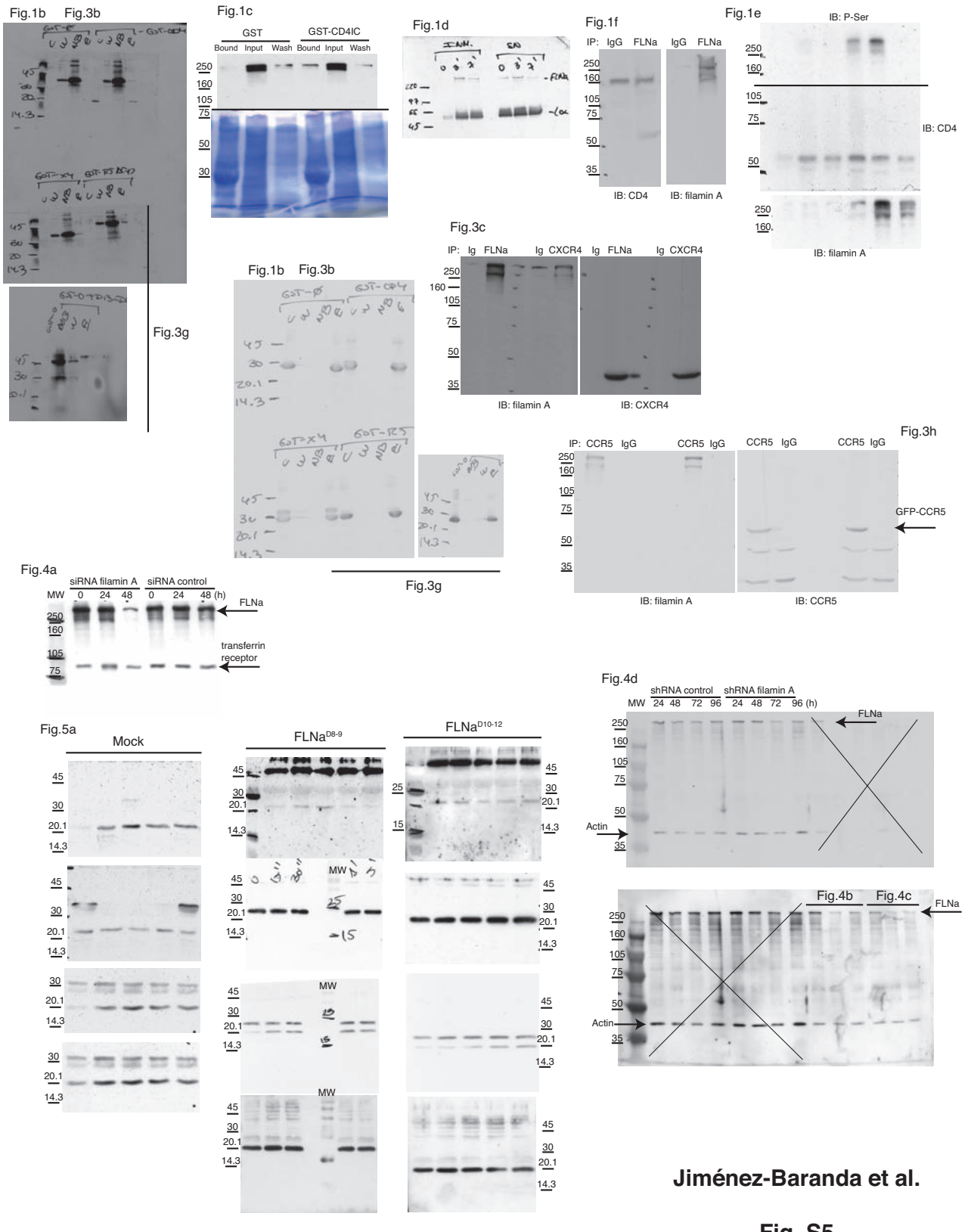

Figure S5. Full blots of figures in the manuscript.

SUPPLEMENTARY METHODS

Antibodies and reagents

Quick Change mutagenesis kit and pfu Turbo DNA polymerase were obtained from Stratagene, pRV-IRESGFP from Genetrix (Madrid, Spain), pGBKT7, pGADT7-Rec, SMART cDNA Synthesis and X-α-Gal from Clontech (Mountain View, California, USA), JetPei from Polyplus Transfection (New York, USA), Ficoll-Hypaque and GST beads from Amersham Biosciences (Little Chalfont, United Kingdom), CLAP protease inhibitor (chymostatin, leupeptin, antipain and pepstatin) from Sigma-Aldrich (St. Louis, Missouri, USA), Y-27632 from Calbiochem (Darmstadt, Germany), M-450 goat anti-mouse magnetic beads from Dynal A.S. (Oslo, Norway), carboxylate microspheres (4.5 μm) and Streptavidin-coated beads (6 μm) from Polysciences Inc. (Warrington, Pennsylvania, USA), anti-CD4 monoclonal antibody for immunoisolation of plasma membrane fragments from Invitrogen-Caltag (Carlsbad, California, USA), anti-CD4 for activation assays (HP2.6) was a gift of F. Sanchez-Madrid (Hospital de la Princesa, Madrid, Spain), the GST-Rhotekin and the GST-PAK from Upstate Biotechnology (Charlottesville, Virginia, USA), anti-filamin-A from Lab Vision (Fremont, California, USA), anti-CD4 intracellular domain, anti-RhoA, anti-Rac and anti-CXCR4 (H118) antibodies from Santa Cruz Biotechnology (Santa Cruz, California, USA), anti-CCR5 (MAB1801) from R&D Systems (Minneapolis, USA), anti-phosphoserine and anti-phospo-cofilin from Biosource (Camarillo, California, USA), anti-cofilin from Cell Signaling Technology (Beverly, Massachusetts, United States), actin-rhodamine from Molecular Probes (Eugene, Oregon, United States), biotin-, peroxidase-, Cy2- and Cy3-labelled secondary antibodies from Jackson ImmunoResearch Laboratories (West

Grove, Pennsylvania, USA), and sheep-anti-gp120 antibody (D7324) from Alto Bio Reagents.

Primers for generation of CD4 mutants.

CD4ICΔ429: 5'-CCCGCCTCAAATGGGGCTTTATGTCTTCTGAAACCGCCC-3´ and 5´-CCCCGGTTTCAGAAGACATAAAGCCCCATTTGAGGCGGG-3´;

CD4ICΔ421: 5´-CCCCTGAAACCGGTGAGGTTACTGGCAGGTCTTCTTCCC-3´and 5´-CCCAAGAAGACCTGCCAGTAACCTCACCGGTTTCAGCCC-3´;

CD4ICΔ416: 5´-CCCCTGGCAGGTCTTCTTTTAACTGAGGAGTCTCTTCCC-3´ and 5´-CCCAAGAGACTCCTCAGTTAAAAGAAGACCTGCCAGCCC-3´;

CD4IC^{C420A,C422A}:5´-CCCCTGAAACCGGTCAGGAGCCTGAGCGGTCTTCTTCTCACTCCC-3´ and 5´-CCCAGTGAGAAGAAGACCGCTCAGGCTCCTCACCGGTTTCAGCCC-3´;

CD4IC$^{412-415A}$: 5´CCCGCAGGTCTTCTTCTCTGCAGCTGCGGCCTTGATCTGCCC-3´, 5´-GGGCAGATCAAGGCCGCAGCTGCAGAGAAGAAGACCTGCGGG-3´, 5´-CCCATGTCTCAGATCAAGGCCGCACTCAGTGAGAAGAAGCCC-3´ and 5´-GGGCTTCTTCTCACTGAGTGCGGCCTTGATCTGAGACATGGG-3´

CD4IC ^{K418A}: 5´- CCCCTCCTCAGTGAGAAGGCTACCTGCCAGTGCCCTCCC-3´and 5´-GGGAGGGCACTGGCAGGTAGCCTTCTCACTGAGGAGGGG-3´

CD4IC $^{E416A,\ K417A}$: 5´-GGGGCACTGGCAGGTCTTCGCTGCACTGAGGAGTCTCTTCCC-3´ and 5´-GGGAAGAGACTCCTCAGTGCAGCGAAGACCTGCCAGTGCCCC-3´

Primers for generation of FLNa fragments and mutants.

FLNa D10: 5'-GCGAATTCTTTGACG CATCCAAA-3' and 5'-GCGGATCCGCCTTGCTGGGGAAGTT-3';

FLNa D8-9: 5’-GCGAATTCCTGGACCTCAGCAAG-3’ and 5’-GCGGATCCGCGG GAACCACGTGGGC-3’;

FLNa D10-12: 5’-GCGAATTCTTTGACGCATCCAAA-3’ and 5’-GCGGATCCCTT GAAAGGACTGCCTGG-3’;

FLNa D13-16: 5’-CGGAATTCACAGATGCGTCCAAG-3’ and 5’-GCCTCGAGCT GCAAGGGGCTTCC-3’;

FLNaD16-20: 5’-CGGAATTCGCCCCGGAGAGGCCC-3’ and 5’-GCGGATTCCCC TAGGGGCCCCAC-3’;

FLNaD20-24: 5’-CGGGATCCCGAAAGAGAGCATCACC-3’ and 5’-GCCTCGAGT CAGGGCACCACAAC-3’;

FLNa D10(F1243S,S1245F): 5’-CCAGCCCGTGCCCAACAGTCCCTTCAAGGCGG ATCCACC-3´ and 5´-GGTGGATCCGCCTTGAAGGGACTGTTGGGCACGGGCTG G-3´

FLNaD10(E1217P): 5’-CCCGGAAGCCCCGCAGGCGAGCAGATCTCCC-3’ and 5´-GGGAGATCTGCTCGCCTGCGGGGCTTCCGGG-3’

Sequences of siRNA duplexes.

FLNa-DUPLEX 1: Sense 5’-CCAACAAGGUCAAAGUAUAUU-3’, antisense 5’-UA UACUUUGACCUUGUUGGUU-3’

FLNa-DUPLEX 2: Sense 5’-GCAGGAGGCUGGCGAGUAUUU-3’, antisense 5’-AU ACUCGCCAGCCUCCUGCUU-3’

FLNa-DUPLEX 3: Sense 5’-UCACAGAAAUUGACCAAGAUU-3’, antisense 5’-UC UUGGUCAAUUUCUGUGAUU

Control-DUPLEX: Sense 5’-CUCUCGCCGUAAUAGCAGUUU-3’, antisense 5’-AC UGCUAUUACGGCGAGAGUU-3’

Cell culture and transfections

Human PBMC were purified on Ficoll-Hypaque gradients and activated for 2 days with 1 μg/ml PHA and 50 ng/ml IL2. MT-2, Jurkat and GFP-CCR5-expressing Jurkat cells[1] were maintained in RPMI 1640, 10% FCS, 1 mM sodium pyruvate, 2 mM L-glutamine, 100 U/ml penicillin and 100 μg/ml streptomycin. HEK-293 cells were maintained in DMEM, 10% FCS, 2 mM L-glutamine and antibiotics; HEK-293-CD4 cells were cultured as for HEK-293, with addition of G418 (1 mg/ml); M2 and A7 cells were maintained as described[2].

M2 and A7 cells were transfected with SRαpuro-CD4 vector; after puromycin selection, resistant clones were infected with recombinant pRV-CXCR4-GFP or pRV-GFP-CCR5 retroviruses[1] and GFP-positive cells selected by sorting in a Coulter Epics Altra (Beckman Coulter, Fullerton, CA). Cells were maintained in G418 and puromycin, and sorted by FACS every two months to maintain CXCR4 and CCR5 expression. Infection with pRV-CXCR4-GFP or pRV-GFP-CCR5 retroviruses was used to generate M2-CXCR4-GFP, M2-GFP-CCR5, A7-CXCR4-GFP and A7-GFP-CCR5 cells. Jurkat cells were infected with pRV-Myc-filamin-A-repeats8-9IRESGFP or pRV-Myc-filamin-A-repeats10-12-IRESGFP retroviruses and transduced cells selected by cell sorting. For RNA interference, cells were Oligofectamine-transfected with each of three double-stranded filamin-A-specific or a control oligonucleotide (see above). In some experiments, cells were re-transfected with full-length filamin-A or the empty vector 24 h after siRNA transfection, and assayed in infection experiments 24 h later. Jurkat cells were also infected with specific shRNA (see above) subcloned in the lentiviral vector pLVTHM (a gift of A. Bernad, CNB. Madrid. Spain). Filamin-A expression was assessed by immunoblotting.

Immunoisolation of plasma membrane fragments

M-450 goat anti-mouse magnetic beads were coated with monoclonal anti-CD4 antibody. Jurkat cells (3 x 10^7) were incubated (4ºC, 2 min) with anti-CD4 beads (bead/cell ratio 1:2) in RPMI with 1% FCS. Bead-cell conjugates were incubated (37ºC) for indicated times, washed once with ice-cold H buffer (10 mM sodium Hepes, pH 7.2, 250 mM sucrose, 2 mM $MgCl_2$, 10 mM NaF, and 1 mM vanadate) and resuspended in 1 ml H buffer containing 0.2 mM pervanadate and CLAP protease inhibitor (100 μM). Cells were nitrogen-cavitated (50 bar, 4ºC, 7 min) using a nitrogen cavitation bomb (Parr Instrument Company, Moline, IL). Homogenate was brought to 10 ml with H buffer, beads retrieved with a magnet, then pelleted by ultracentrifugation (100,000 xg, 4ºC, 20 min). Beads and cell pellets were analyzed in immunoblot.

Calcium mobilization

CXCR4-GFP- and GFP-CCR5-expressing M2 and A7 cells (2 x 10^6) were incubated (15 min, 37ºC) with Fluo-3,AM (Molecular Probes) (300 mM in DMSO, 10 μl/10^6 cells). Cells were then resuspended in complete medium containing 2 mM $CaCl_2$, and maintained at 37ºC until CXCL12 or CCL5 addition (20 nM, Peprotech, Rocky Hill, New Jersey, USA). Ca^{2+} release was determined (37ºC, 525 nm) in an EPICS XL cytometer (Beckman Coulter Inc., Fullerton, California, USA).

Chemotaxis assays

To analyze filamin-A function in CXCR4-induced chemotaxis, MT-2 cells were transiently transfected with GFP, GFP-$FLNa^{D8-9}$ or GFP-$FLNa^{D10-12}$ and green cells sorted by FACS (Beckman Coulter Inc.). After 24 h, 3 x 10^5 serum-starved cells were seeded in the upper chamber of 0.8 μm transwells (Cultek, Madrid, Spain); lower chambers were filled with serum-free medium alone or containing CXCL12 (25 nM). After incubation (4 h, 37ºC), we estimated the cell number in the lower chamber by

FACS. The migration index was calculated as the number of cells that migrate to CXCL12 relative to those that migrate in basal medium.

F-actin formation

To analyze gp120-induced F-actin formation, $FLNa^{D10-12}$- or $FLNa^{D8-9}$-expressing Jurkat cells (2 x 10^5) in RPMI 1640/1% FCS/10 mM Hepes (pH 7.5), prewarmed at 37ºC, were stimulated with gp120-beads at indicated times. Aliquots were taken of the cells before gp120 stimulation to determine basal F-actin. Cells were fixed immediately with paraformaldehide, permeabilized and stained (15 min, 4ºC) with FITC-phalloidin (Molecular Probes). Phalloidin incorporation was measured by flow cytometry (LSR, Beckton Dickinson, Franklin Lakes, New Jersey, USA). A similar protocol was followed to determine F-actin in response to CXCL12 stimulation (50 nM, 37ºC) in M2- and A7-CXCR4-GFP cells.

gp120 bead preparation

Streptavidin-coated beads (6 μm) were incubated sequentially at 4ºC with biotinylated rabbit anti-sheep IgG Fab´2 fragment, sheep-anti-gp120 antibody and recombinant $gp120_{IIIB}$ (NIH AIDS Research and Reference Reagent Program; Division of AIDS, NIAID, NIH). PHA-activated human peripheral blood mononuclear cells (2 x 10^6) or Jurkat cells retrovirally transduced with mock, filamin-A repeat 10-12 or repeat 8-9 fragments (5 x 10^6) were stimulated with gp120 beads (ratio 2:1 for PBL, 1:1 for Jurkat). Cell extracts were analyzed for active RhoA and Rac by immunoprecipitation with GST-Rhotekin and GST-PAK binding domains, respectively, or immunoblotted with anti-RhoA, -Rac, -phosphoserine, -phospo-cofilin, -cofilin, or -filamin-A antibodies.

Env-induced cell-cell fusion

Cell-cell fusion assays were performed as described[3]. Basically, HIV-1env_{IIIB} was introduced in effector HEK-293 cells by infection (1 h, 37ºC) with recombinant vaccinia virus. As target cells, we used CD4-expressing HEK-293 transfected with pSC-luc plasmid harbouring the firefly luciferase gene under the control of the vaccinia virus 7.5 promoter and the promoterless renilla luciferase plasmid. Where indicated, these cells were also transfected with an empty vector, $FLNa^{D10-12}$, $FLNa^{D8-9}$, $FLNa^{D10(F1243S,S1245F)}$, RhoA-GFP, RhoAN19-GFP, Rac-GFP, RacN17-GFP, PAK-1, or PAK-DN mutant (a gift of M.A. del Pozo, Centro Nacional de Investigaciones Cardiovasculares, Madrid, Spain). In some experiments, target cells were pretreated with vehicle, the ROCK inhibitor Y-27632 (10 μM, Calbiochem) or the CXCR4 antagonist AMD3100 (10 μM, Sigma-Aldrich) before mixing with effector cells. For siRNA experiments, cells were co-transfected with each of the FLNa-specific or scrambled siRNA duplexes (100 nM; Dharmacon, Lafayette, Colorado, USA), and a Cy3-labeled non-specific duplex control to determine transfection efficiency by FACS. Silencing was confirmed 48 h post-transfection by immunoblot.

Fusion was performed by mixing 10^5 effector cells cultured in 100 μg/ml rifampicin with 2 x 10^5 target cells (6 h, 37ºC), and firefly and renilla luciferase activities measured in cell lysates (25 mM Tris-phosphate, pH 7.8, 1% Triton X-100, 1 mM EDTA, 1 mM DTT, 8 mM $MgCl_2$, 15% glycerol).

Computational analyses

Complete protein sequences of CD4_HUMAN (UniProt) and Filamin-A were used independently as queries against NCBI databases, using PSI-BLAST to retrieve all available sequences. Multiple alignments shown here were generated using T-COFFEE[4] and checked manually.

Molecular modelling

We generated a structural model of filamin-A repeat 10 based on the available unbounded structure of repeat 17 (not shown). The model was based on the published crystal structure of the filamin-A repeat 17-GPIbα complex (PDB code 2BP3) and obtained using WHATIF[4] and SWISS-MODEL[5]. The model was evaluated using PSQS (http://www1.jcsg.org/psqs/) and WHATIF.

Supplementary references:

1. Gómez-Moutón, C. et al. Dynamic redistribution of raft domains as an organizing platform for signaling during cell chemotaxis. J. Cell Biol. **164**, 759-768 (2004).

2. Cunningham, C. et al. Actin-binding protein requirement for cortical stability and efficient locomotion. Science **255**, 325-327 (1992).

3. del Real, G. et al. Blocking of HIV-1 infection by targeting CD4 to non-raft membrane domains. J. Exp. Med. **196**, 293-301 (2002).

4. Notredame, C., Higgins, D.G. & Heringa, J. T-Coffee: A novel method for fast and accurate multiple sequence alignment. *J Mol Biol* 302, 205-217 (2000).

5. Schwede, T., Kopp, J., Guex, N. & Peitsch, M.C. SWISS-MODEL: An automated protein homology-modeling server. *Nucleic Acids Res* 31, 3381-3385 (2003).